Supplementary information

Contents:

Information

Tables

Figures

1. Instrumentation details

Synthesized nanomaterials were characterized with relevant techniques to understand their bonding, structure, size, and morphology. Powder X-ray diffraction (PAN analytical X-PRT PRO) with 1.5406 A° wavelengths of Cu Kα radiation. Fourier Transform Infrared Spectroscopy (Agilent Cary 630 FTIR) was used to identify bonding *via* the emission and absorption process. Surface charge and stability were calculated using Zeta-sizer (Malvern). Raman spectrometer (RMP-500 Series Probe) was used to analyse chemical structure of the nanomaterial. The band gap was calculated from a UV spectrophotometer using Kubelka-munk function. The surface morphology and element distribution of nanocatalysts were observed HR-TEM, SEM-EDS (Hitachi S-4800), and the surface element distribution of the catalyst were observed by an energy spectrometer matched with a scanning electron microscope. The chemical bonding state and surface porosity of nanoparticles were studied by XPS (Thermo Scientific ESCALAB250Xi) and BET (measured by a spectrometer). The band gap of nanocatalysts were measured by the UV−vis (Shimadzu UV 3600) spectrophotometer within the wavelength of 200−700 nm.

2. Statistical analysis

The graphs plotted in kinetics study, and statistical treatment of experimental data for removal of HQ and 4-NP by synthesized nanocomposites were performed empirically from asymptotical analysis by Sigma Plot Systat 14.0 and Origin software 8.5. The good agreement of result was shown for triplicate samples and "Microsoft Excel" was used for the calculation of standard deviation. The significance of experimental data was analysed by *p*-values, beta coefficient (R^2), and chi square. Fit equations were used for kinetics and adsorption data.

3. Static Photocatalytic degradation study

In this study, the photocatalytic performance of the prepared nanocatalysts was assessed by degrading HQ and 4-NP in sunlight. To begin, a highly concentrated stock solution of 100 mgL^{-1} was prepared for targeted pollutants using distilled water as solvent. Batch experiments were conducted for the optimization of various reaction parameters such as pollutant concentration (10-50 mgL^{-1}), catalyst dose (10-30 mg), irradiation source (dark, artificial bulb and sunlight) and pH (3-11). The dark and blank study was also conducted having no catalyst, to determine the adsorption capacity and photocatalysis alone respectively. A pyranometer was used to detect the solar intensity while photocatalytic tests were carried out in direct sunlight. The average temperature and solar intensity, which were determined to be 550 ± 175 Wm^{-2}

Ag@ZnHCF-rGO					rGO				
S.no.	**2Θ**	**FWHM**	**d-spacing (A^0)**	**Rel. Int. [%]**	**S.no.**	**2Θ**	**FWHM**	**d-spacing (A^0)**	**hkl values**
1.	23.45	0.4015	3.79359	8.43	1.	24.10	9.8705	3.688	(100)
2.	29.74	0.3346	3.00337	16.47	2.	58.08	30.067	1.586	(210)
3.	31.55	0.1338	2.83570	70.51					
4.	34.27	0.2342	2.61615	56.92					
5.	35.11	0.2342	2.55543	48.87					
6.	36.02	0.2175	0.79337	100.00					
7.	38.91	0.2676	2.31444	12.04					

(ranging: 160–850) and 42 ± 1.5 °C (range: 32.0–45.0), respectively, during the degradation study, which took place at the MNIT campus in Rajasthan in April from 10:30 am to 3:30 pm. To confirm the results, triplet repetitions of the experiments were carried out. Both citrate (0.1 M trisodium citrate + 0.1 M citric acid) and borax (0.1 M sodium hydroxide + 0.025 M borax) buffers were employed to keep the pH level stable. During the reaction process, 3 mL sample was collected at certain intervals and was evaluated after removing the nanoparticle using the syringe filter (AXIVA Nylon filters having size 25 mm with micron rating 0.2 µm). To examine the degradation efficiency of pollutants, the absorbance of the targeted pollutants at their ƛ max were examined employing a UV–Vis Spectrophotometer (Shimadzu UV 1900). Before the experiment calibration has been carried out for different concentrations of HQ and 4-NP (10-50 mg L^{-1}). The spectra have been plotted for various concentrations against absorbance and then through this calibration curve, unknown concentration of pollutants after the experiment has been deduced. The degradation efficiency was determined using the following formula:

$$\text{Degradation efficiency (\%)} = C_o - \frac{C_t}{C_o} * 100$$

where the variable C_o represents the initial concentration of the pollutants and the value of variable C_t refers to the concentration of the pollutants afterwards to degradation under sunlight.

Table 1s. Detailed information of 2Θ value, FWHM, d-spacing and hkl for synthesised nanomaterials.

8.	42.67	0.4015	2.11872	8.10
9.	47.41	0.2676	1.91741	17.98
10	56.47	0.3011	0.2933	38.23
11.	62.11	0.2676	1.49431	18.89
12.	62.71	0.4015	1.48141	21.29
13.	67.75	0.4684	1.38305	20.15
14.	68.95	0.4015	1.36182	9.99

Table 2s. Adsorption isotherm (Langmuir, Freundlich, DR, Temkin) resulted from different R^2 and p values of Ag@ZnHCF-rGO, Ag@ZnHCF, ZnHCF and rGO for HQ

	Langmuir		**Freundlich**		**DR**		**Temkin**	
Catalyst	**R^2**	**p**	**R^2**	**p**	**R^2**	**p**	**R^2**	**p**
Ag@ZnHCF-rGO	0.97	0.031	0.96	0.022	0.82	0.022	0.83	0.029
Ag@ZnHCF	0.98	0.025	0.89	0.026	0.88	0.026	0.92	0.026
ZnHCF	0.97	0.035	0.95	0.025	0.84	0.022	0.84	0.025
rGO	0.97	0.026	0.82	0.028	0.82	0.024	0.82	0.026

Table 3s. Adsorption isotherm (Langmuir, Freundlich, DR, Temkin) resulted from different R^2 and p values of Ag@ZnHCF-rGO, Ag@ZnHCF, ZnHCF and rGO for 4-NP

	Langmuir		**Freundlich**		**DR**		**Temkin**	
Catalyst	**R^2**	**p**	**R^2**	**p**	**R^2**	**p**	**R^2**	**p**
Ag@ZnHCF-rGO	0.98	0.022	0.95	0.025	0.89	0.032	0.91	0.043
Ag@ZnHCF	0.97	0.015	0.88	0.027	0.91	0.005	0.87	0.0034
ZnHCF	0.97	0.031	0.93	0.025	0.84	0.023	0.82	0.016
rGO	0.98	0.022	0.86	0.018	0.88	0.026	0.81	0.025

Table 4s. The reaction rate constant values between reactive oxidative species and specific quenchers have been described below:

a) HQ

Quenchers	C_t/C_o	ln C_t/C_o	K (min^{-1})
Control	0.05	-2.99573	0.016643
t-BuOH	0.7	-0.35667	0.001982
p-BZQ	0.4	-0.91629	0.005091
Na_2EDTA	0.2	-1.60944	0.008941

b) 4-NP

Quenchers	C_t/C_o	ln C_t/C_o	K (min^{-1})
Control	0.12	-2.12026	0.008834
t-BuOH	0.75	-0.28768	0.001199
p-BZQ	0.6	-0.51083	0.002128
Na_2EDTA	0.43	-0.84397	0.003517

Table 5s. LD_{50} values for HQ, 4-NP and the intermediates formed by their photocatalytic breakdown. (taken from ChemSpider, Web Science as a search engine)

S.no.	Metabolite	LD_{50} value
1.	4-nonylphenol	1,300 - 2,000 mg/kg
2.	phthalic acid	7900 mg/kg in rats
3.	3-hydroxy-2,3-carboxylic acid	Not available
1.	HQ	300-400 mg/kg in rats
2.	Maleic acid	708 mg/kg.
3.	Succinic acid	2,260 mg/kg
4.	4-hydroxy muconic semialdehyde	Not available

4. Mass-normalized rate constant:

Mass-normalized rate constant:

$K_{normalized}$ = k /catalyst loading

With regard to catalyst mass, the photocatalytic activity has now been adjusted. The catalyst loading used in this study (20 mg in 10 mL) corresponds to 2 gL^{-1}. As a result, mass-normalised rate constants (k/m) were computed. In comparison to the binary and individual components, the Ag@ZnHCF-rGO nanocomposite has the highest normalized activity (0.0097 $min^{-1}g^{-1}$ for HQ and 0.00425 $min^{-1}g^{-1}$ for 4-NP), demonstrating its better intrinsic catalytic efficiency as shown in table 6s.

Table 6s: Values of mass-normalized rate constants for targeted pollutants by synthesized catalysts

Catalyst	K (HQ) (min^{-1})	k/m (HQ) (min^{-1} g^{-1})	k(4-NP) (min^{-1})	k/m (4-NP) (min^{-1} g^{-1})

Ag@ZnHCF-rGO	0.0194	0.0097	0.0085	0.00425
Ag@ZnHCF	0.012	0.0060	0.0044	0.0022
ZnHCF	0.008	0.0040	0.004	0.0020
rGO	0.007	0.0035	0.0033	0.00165

Pollutants	Radiation source	TOC initial (mgL^{-1})	TOC final (mgL^{-1})	Mineralisation rate (%)
HQ	Sunlight	67.827	16.134	76.21
4-NP	Sunlight	82.701	22.546	72.73

5. Numerical band-edge calculation (Mulliken electronegativity theory)

Given (measured / known) for Ag@ZnHCF-rGO:

- Optical band gap: $E_g = 1.8$ eV (Kubelka-Munk).
- Adopted Mulliken electronegativity for the composite: $X = 5.8$ eV.
- Energy of free electron on hydrogen scale: $E_e = 4.50$ eV.

Formulas (potentials **vs NHE**):

$E_{CB} = X - E_e - 0.5\,E_g$ and $E_{VB} = E_{CB} + E_g$ Step-by-step arithmetic:

1.Compute half the band gap:

$0.5 \times E_g = 0.5 \times 1.90 = 0.95$ eV.

1. $E_{CB} = X - E_e - 0.5E_g = 5.8 - 4.50 - 0.95.$
   $\boxed{E_{CB} = 0.40 \text{ V vs NHE}}$

2. $E_{VB} = E_{CB} + E_g = 0.40 + 1.8.$

$\boxed{E_{VB} = 2.20 \text{ V vs NHE}}$

Table 7s: Mineralisation efficiency of the Ag@ZnHCF-rGO photocatalyst as evaluated by TOC analysis for HQ and 4-NP under solar irradiation

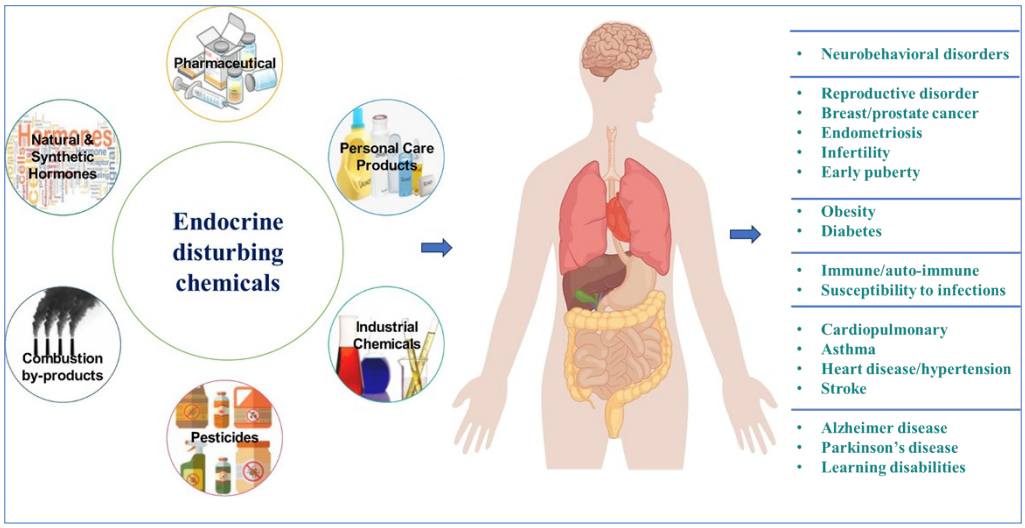

Figure 1s. Sources and toxic effects of endocrine disturbing chemicals on humans

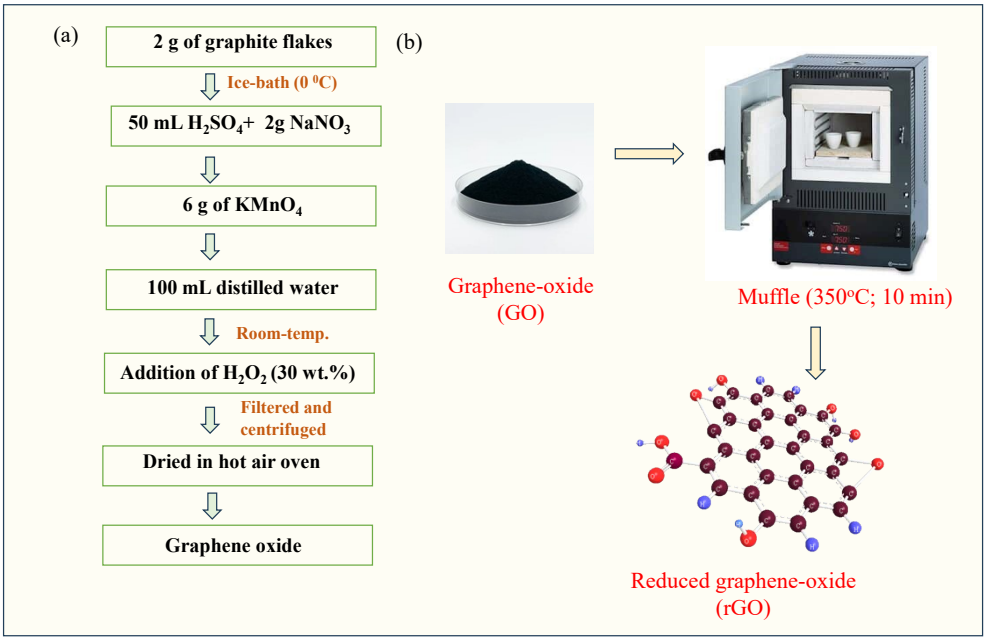

Figure 2s. Schematic representation for the synthesis of (a) GO via Modified Hummer's method and (b) rGO via thermal reduction

\\

Figure 3s. Preparation of leaf extract and its role in nanoparticle synthesis

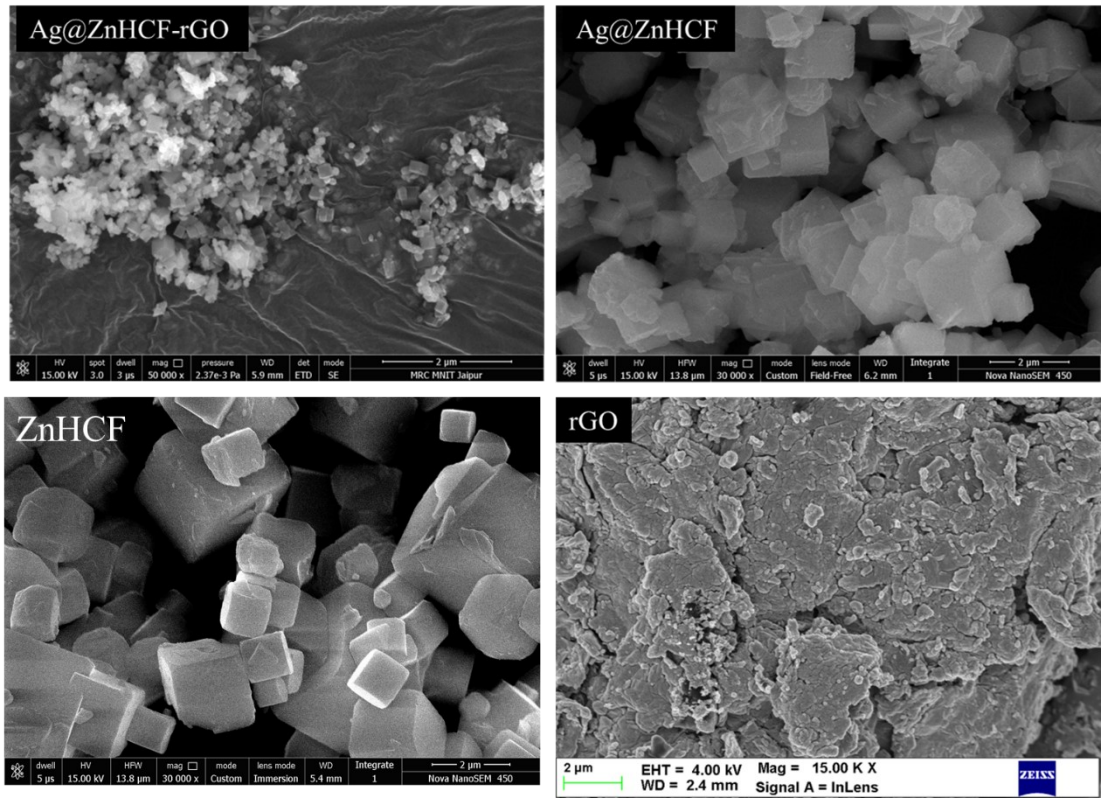

Figure 4s. FE-SEM images of Ag@ZnHCF-rGO, Ag@ZnHCF, ZnHCF, and rGO (Scale:2 µm)

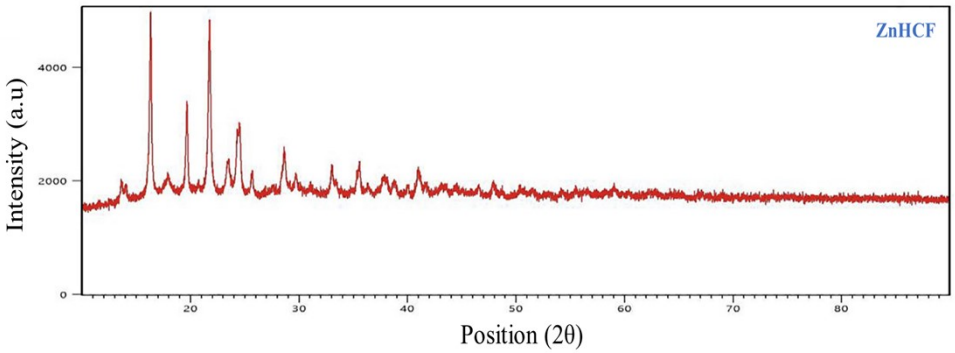

Figure 5s. P-XRD spectra of ZnHCF

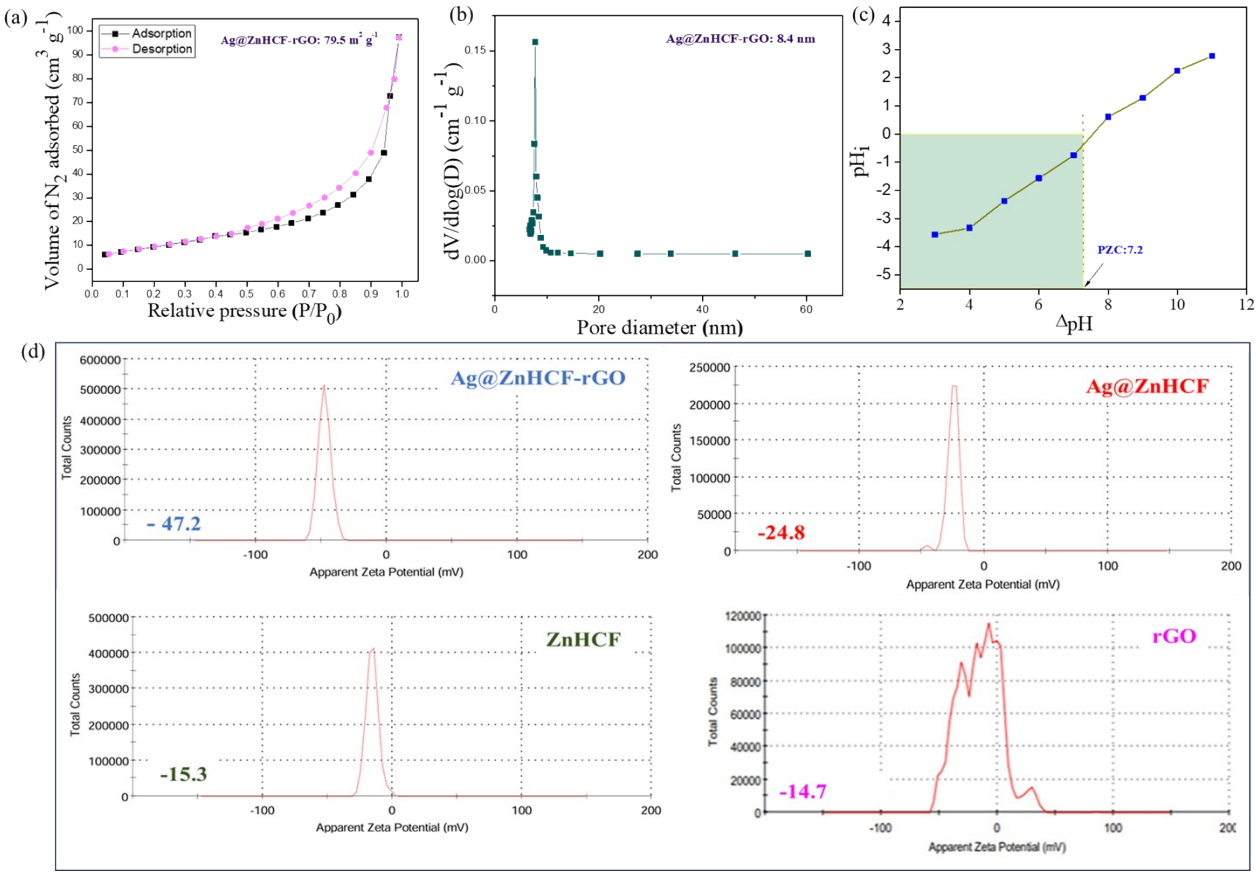

Figure 6s. BET isotherms (b) BHJ plots of Ag@ZnHCF-rGO nanocomposite; (c-d) PZC calculations and Zeta Potential of synthesized catalysts

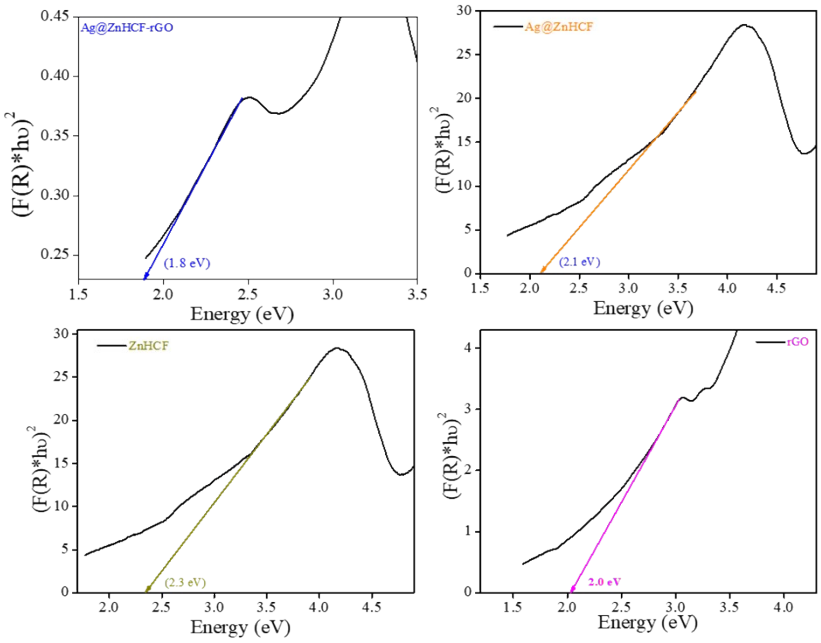

Figure 7s. Determination of band gap via Kubelka-Munk function for synthesized catalysts

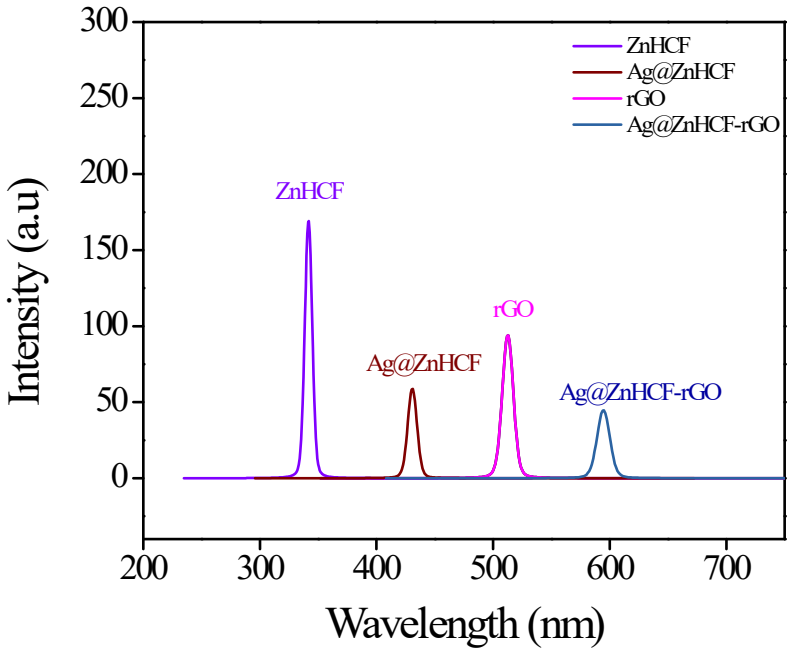

Figure 8s: Photoluminescence (PL) spectra of all the synthesized catalysts

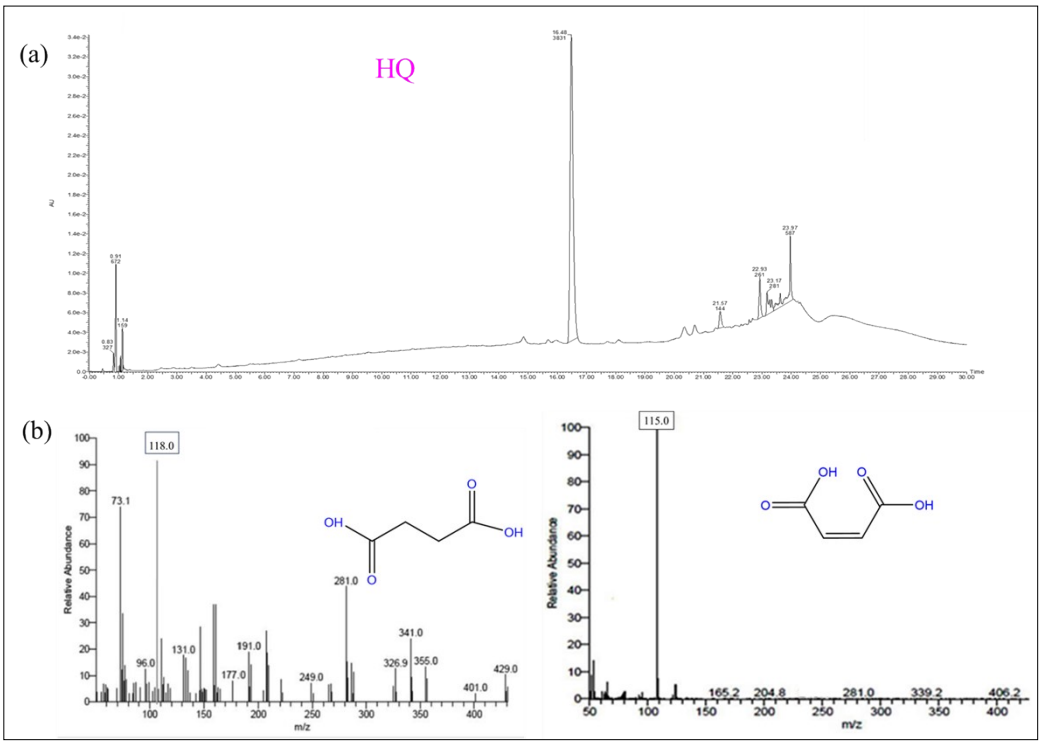

Figure 9s. (a) Total Ion chromatogram and (b) Mass spectra of degraded HQ

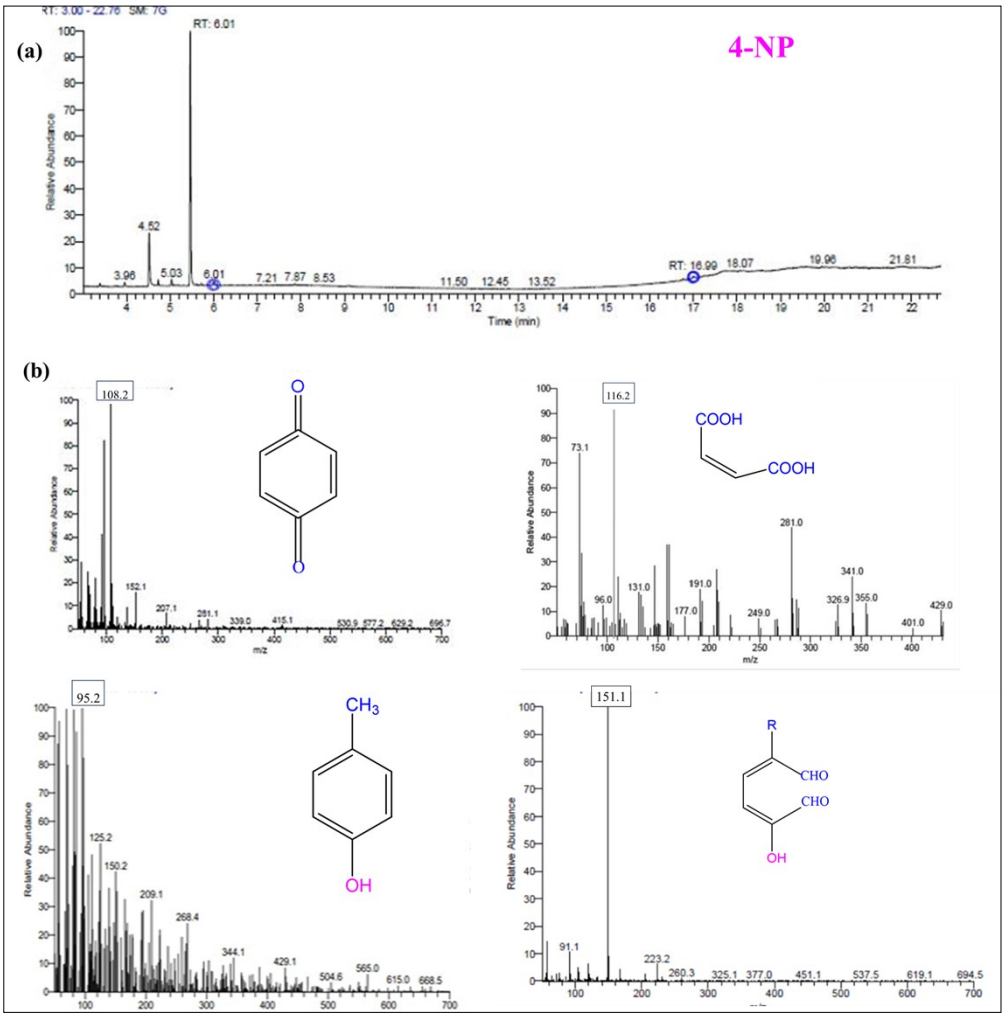

Figure 10s. (a) Total Ion chromatogram and (b) Mass spectra of degraded 4-NP

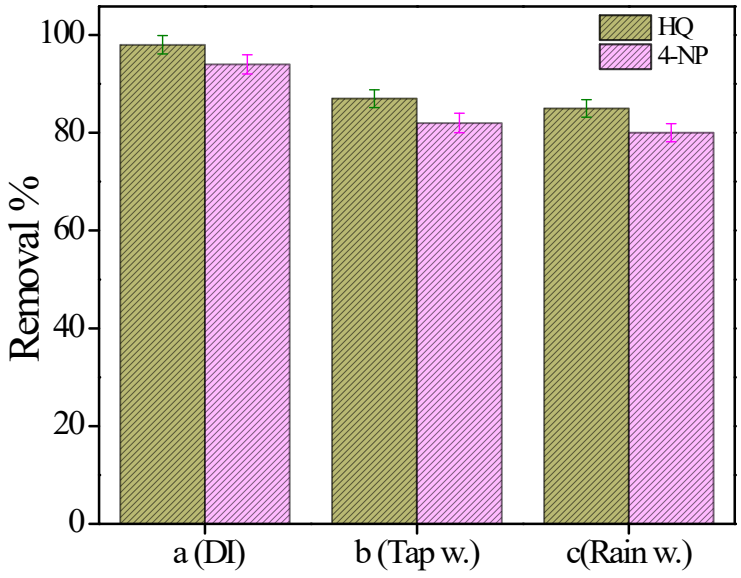

Figure 11s. The efficacy of HQ and 4-NP removal from spiked wastewater samples (a) DI water, (b) tap water (c) rain water

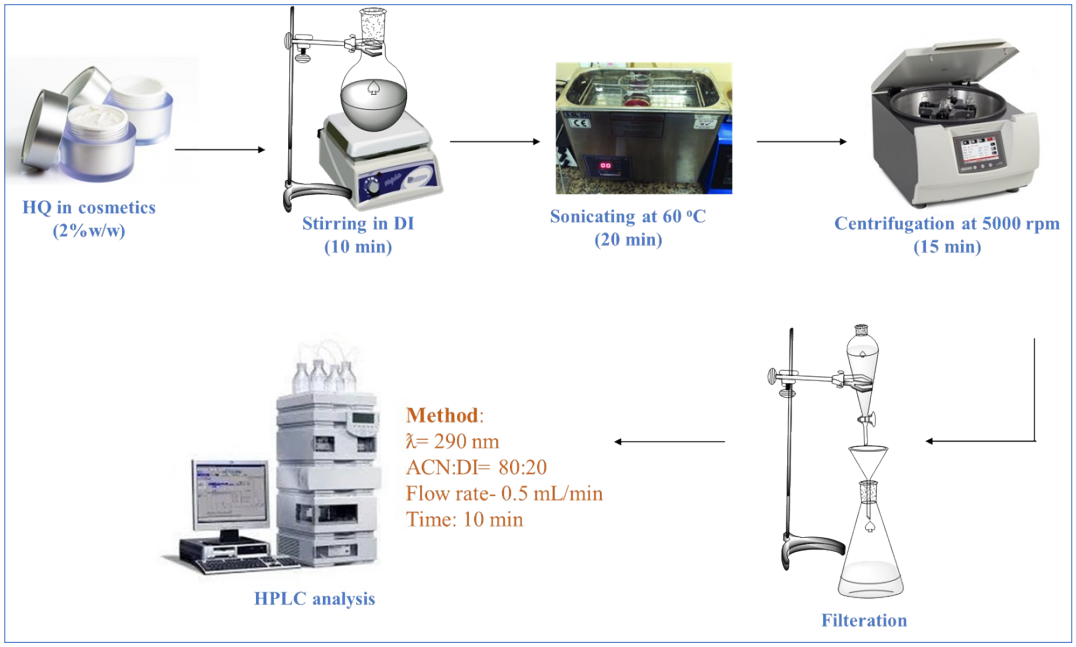

Figure 12s. Schematic representation of the analysis and degradation of HQ from cosmetics via HPLC